



# Characterization of complete Currarino syndrome in pediatrics—a comparison between CT and MRI

Jing Chen<sup>1,2#^</sup>, Nannan Zheng<sup>1,3#</sup>, Chunxiang Wang<sup>2</sup>, Jianbo Shao<sup>3</sup>, Xin Qi<sup>2</sup>, Yingjie Xie<sup>2</sup>, Quan Zhang<sup>1^</sup>

<sup>1</sup>Department of Medical Imaging, Tianjin Medical University General Hospital, Tianjin, China; <sup>2</sup>Department of Medical Imaging, Tianjin Children's Hospital (Children's Hospital of Tianjin University), Tianjin, China; <sup>3</sup>Department of Imaging Center, Wuhan Children's Hospital (Wuhan Maternal and Child Healthcare Hospital), Huazhong University of Science and Technology, Wuhan, China

*Contributions:* (I) Conception and design: J Chen; (II) Administrative support: C Wang, J Shao, Q Zhang; (III) Provision of study materials or patients: N Zheng, X Qi, Y Xie; (IV) Collection and assembly of data: J Chen, N Zheng; (V) Data analysis and interpretation: J Chen, Q Zhang; (VI) Manuscript writing: All authors; (VII) Final approval of manuscript: All authors.

<sup>#</sup>These authors contributed equally to this work.

*Correspondence to:* Quan Zhang. Department of Medical Imaging, Tianjin Medical University General Hospital, No. 154, Anshan Road, Heping District, Tianjin 300052, China. Email: quanzhang@tmu.edu.cn.

**Background:** This study sought to analyze the computed tomography (CT) and magnetic resonance imaging (MRI) characteristics of the classical triad elements and the associated anomalies in pediatric complete Currarino syndrome (CS) to evaluate the advantages and disadvantages of the 2 different imaging methods in displaying the abnormalities of this disease.

**Methods:** The clinical and radiological features of 32 pediatric patients with complete CS diagnosed histologically and/or radiologically were retrospectively analyzed.

**Results:** All 32 complete CS patients presented with the classical triad of congenital anorectal malformation (ARM), sacral agenesis, and presacral mass. Anal atresia, which is the most common congenital ARM, was observed in 19 of the 32 patients (59.4%). Sacral agenesis was mainly type IV (75%). Among the presacral masses, true tumors and pseudotumors accounted for about half each. All of the 15 true tumors were presacral teratomas. Twenty-five patients had associated anomalies, including tethered cord, filum lipoma, and hydronephrosis. Twenty-four patients underwent both CT and MRI examinations. While CT was better than MRI in displaying sacral anomaly ( $P < 0.05$ ), MRI was more sensitive than CT at detecting presacral mass, spinal dysraphism, and congenital anal atresia ( $P < 0.05$ ).

**Conclusions:** CT and MRI have different efficiencies at displaying the abnormalities of the complete CS. As a non-invasive method, MRI has significant advantages in diagnosing complete CS, especially in revealing the details of ARM, presacral mass, and associated spinal dysraphism.

**Keywords:** Currarino syndrome (CS); sacral agenesis; congenital anal atresia; magnetic resonance imaging (MRI); computed tomography (CT)

Submitted Nov 18, 2021. Accepted for publication Jan 05, 2022.

doi: 10.21037/atm-21-6572

View this article at: <https://dx.doi.org/10.21037/atm-21-6572>

<sup>^</sup> ORCID: Jing Chen, 0000-0002-1181-5606; Quan Zhang, 0000-0002-9776-2401.

## Introduction

Currarino syndrome (CS), which is a rare triad of a congenital anorectal malformation (ARM), sacral anomaly, and presacral mass, was first described by Currarino *et al.* in 1981, and initially named the “Currarino triad” (1). In 2000, Belloni *et al.* found that in addition to the 3 main anomalies mentioned above, CS could also be accompanied by other abnormalities, such as urogenital system malformations, microcephaly, and spinal dysraphism (2,3). It was thus renamed “Currarino syndrome”.

Patients who suffer from CS exhibit phenotypic variability. Early diagnosis and treatment are key to improving the prognosis of patients with CS. The clinical manifestations and imaging findings of patients with CS vary. Apart from the classical triad elements of the complete CS subtype, there is an incomplete CS subtype without 1 or 2 of the main anomalies (4). As radiological findings cannot correctly diagnose the incomplete CS subtype, these patients often need to undergo genetic examinations to obtain an accurate diagnosis. Thus, in this study, we only discuss the imaging manifestations for complete CS.

Radiological findings are important in detecting the abnormalities of CS. However, the imaging features of pediatric patients with complete CS are complex and diverse, and presently, there is no imaging evaluation guidelines based on a large number of cases. In the past, ultrasonography combined with X-ray or fluoroscopy examination were usually used to diagnose complete CS. Ultrasonography can detect large presacral masses, but it is often unable to determine the nature of these masses. X-ray or fluoroscopy examinations only have certain diagnostic value for sacral deformity. X-ray plain film of sacrum can show the morphology of sacrum, but this method has some limitations. When there is extensive gas accumulation in the intestine, the interference of intestinal gas may affect the display of sacral morphology. Therefore, nowadays X-ray plain film of sacrum is no longer used to evaluate complete CS. Thus, these examination methods have great limitations in diagnosing complete CS. We hope to reduce the choices of examinations and use the lowest radiation dose possible to make a correct diagnosis of complete CS.

In this study, we present a series of 32 cases with complete CS who underwent computed tomography (CT) and/or magnetic resonance imaging (MRI) scans to evaluate the advantages and disadvantages of the CT and MRI methods in displaying the abnormalities of this disease.

We present the following article in accordance with the MDAR checklist (available at <https://atm.amegroups.com/article/view/10.21037/atm-21-6572/rc>).

## Methods

All procedures performed in this study involving human participants were in accordance with the Declaration of Helsinki (as revised in 2013). The study was approved by the Ethics Committee of Tianjin Children’s Hospital (No. 2016021) and Wuhan Children’s Hospital (No. 2020RO15-E01). Individual consent for this retrospective analysis was waived.

## Patients

Thirty-two pediatric patients (from Tianjin Children’s Hospital and Wuhan Children’s Hospital) with complete CS diagnosed histologically and/or radiologically from July 2012 to August 2020 participated in this study. Of the 32 complete CS patients, 12 were male (37.5%) and 20 were female (62.5%). The patients had a median age of 28 days (range, 1 day to 14 years). The clinical features of the 32 patients are displayed in *Table 1*.

## Clinical and imaging data collection

The clinical data included demographic information and primary clinical symptoms. Lumbosacral CT scans were acquired using 3 CT scanners (from GE Healthcare, Siemens Healthcare, and Philips Healthcare) with the following parameters: 120 kV, 240–260 mA, 5-mm slice thickness, a 1.25-mm reconstruction, and a CT dose index (CTDI) vol of 7–14 mGy.

Pelvic MRI was performed with 1.5-Tesla or 3.0-Tesla equipment (from GE Healthcare and Siemens Healthcare). The MRI protocol comprised sagittal and axial T1-weighted spin-echo (SE) sequences, T2-weighted fast spin-echo (FSE) sequences, and post-contrast T1-weighted SE sequences. T1-weighted fat-saturated turbo SE sequences were performed when a short T1 signal intensity lesion was detected.

Newborns were wrapped tightly after feeding to promote sleep. Patients, who could not cooperate to complete the MRI examination, orally took 0.80 mL/kg per body mass of 6.5% chloral hydrate before the examination to control movement.

**Table 1** Summary of clinical characteristics (n=32)

Characteristics	Number of patients (%)
Sex	
Boy	12 (37.5)
Girl	20 (62.5)
Age	
Neonate ( $\leq 28$ days)	16 (50.0)
Infant (28 days to 3 years)	13 (40.6)
$>3$ years	3 (9.4)
Symptom	
No meconium excretion after birth	7 (21.9)
Dysporia	12 (37.5)
Abdominal distension	12 (37.5)
Vomiting	7 (21.9)
Abdominal pain	1 (3.1)

### Radiological assessments

All the CT/MRI images were evaluated by 2 experienced pediatric radiologists with  $>5$  years' experience in pediatric radiologic diagnosis. The imaging indices, including the shape of lumbosacral vertebrae, calcification in the presacral mass, the type of congenital anal atresia, the component of presacral mass, and associated anomalies of the spinal and urogenital system, were assessed by reviewing the CT and MRI images. In addition, for the 24 cases who underwent both lumbosacral CT and pelvic MRI examination, a chi-square test was conducted to compare the detection rate of CT and MRI in abnormalities.

### Statistical analysis

The Statistical Parametric Mapping (SPM) 25 statistical package was used for the statistical analysis. The Chi-square test was performed, and a significance level of 5% was used.

## Results

### Patient characteristics

Among the 32 complete CS patients, 16 (50%) were diagnosed at birth or in the neonatal period, 13 (40.6%) were diagnosed from 28 days to 3 years old, and 3 (9.4%) were diagnosed after the age of 3 years old. The vast majority

( $>90\%$ ) were diagnosed before the age of 3 years old. Children with anal atresia, especially those without a fistula, were usually diagnosed in the neonatal period ( $\leq 28$  days).

The clinical manifestations included no meconium excretion after birth (7 cases, 21.9%), dysporia (12 cases, 37.5%), abdominal distension (12 cases; 37.5%), vomiting (7 cases, 21.9%), and abdominal pain (1 case, 3.1%). 7 of the 32 patients had 2 kinds of symptoms at the same time.

### Distribution of the classical triad elements of complete CS

Among the 32 patients, 3 patients only underwent lumbosacral examinations CT and 5 patients only underwent pelvic MRI examinations, while 24 patients underwent both CT and MRI examinations. All of the 32 patients presented with the classical triad elements. The types and prevalence of congenital ARM, sacral agenesis, and presacral mass are displayed in *Table 2*.

Congenital ARM consists of anal atresia, anal stenosis, and Hirschsprung disease. Among the 32 patients, 19 (59.4%) had anal atresia (see *Figure 1*), including 12 cases with a fistula, 12 (37.5%) cases with anal stenosis, and 1 (3.1%) case was Hirschsprung disease.

Sacral agenesis was classified into 5 types using Pang's classification system, under which type I refers to total sacral agenesis with lumbar vertebra involvement, type II refers to total sacral agenesis without lumbar vertebra involvement, type III refers to total subtotal sacral agenesis with S1 present, type IV refers to total hemisacrum, and type V refers to total coccyx agenesis (5). Among the 32 patients, type IV was the most common (24 cases, 75%) (see *Figures 1-4*), followed by type III (4 cases, 12.5%), type V (3 cases, 9.4%) (see *Figure 5*), and type II (1 case, 3.1%).

The presacral masses included 14 (43.8%) teratomas [13 mature teratoma (see *Figure 2*) and 1 immature teratoma], 8 (25%) anterior meningoceles (see *Figure 2*), 4 (12.5%) anterior myelomeningoceles, 5 (15.6%) anterior lipomeningoceles (see *Figure 4*), and 1 mature teratoma combined with an anterior meningocele.

### Associated anomalies of complete CS

Twenty-five (78.1%) of the 32 patients had associated anomalies in addition to the classical triad elements listed in *Table 3*. Eight patients (32%) had 2 or more associated abnormalities. Among all the types of associated anomalies, tethered cord (see *Figure 3*) accounted for more than half of

**Table 2** Distribution of classical triad elements of complete Currarino syndrome (n=32)

Type of anomaly	Number of patients (%)
Congenital anorectal malformation	
Anal atresia	19 (59.4)
Anal atresia without a fistula	7 (21.9)
Anal atresia with a fistula	12 (37.5)
Anal stenosis	12 (37.5)
Hirschsprung's disease	1 (3.1)
Sacral anomaly	
Type I	0
Type II	1 (3.1)
Type III	4 (12.5)
Type IV	24 (75)
Type V	3 (9.4)
Presacral mass	
Teratoma	14 (43.8)
Mature teratoma	13 (40.86)
Immature teratoma	1 (3.1)
Anterior meningocele	8 (25)
Anterior myelomeningocele	4 (12.5)
Anterior lipomeningocele	5 (15.6)
Mature teratoma + anterior meningocele	1 (3.1)

those anomalies (59.4%), followed by filum lipoma (40.9%) (see *Figures 2-4*), and hydronephrosis (15.6%). It should be noted that no comprehensive review was conducted of other organ systems.

#### ***Comparison between CT and MRI in detecting the classical triad elements and associated anomalies***

MRI was more sensitive than CT at detecting presacral mass, spinal dysraphism, and congenital anal atresia ( $P < 0.05$ ). CT was better than MRI in displaying sacral anomaly ( $P < 0.05$ ; see *Table 4*).

#### **Discussion**

Complete CS can be classified as familial or sporadic. Familial CS is considered an autosomal dominant condition.

MNX1 mapped to 7q36, previously named HLXB9, is the main causative gene of familial CS (6,7). More than 80 mutations at the MNX1 locus have been described thus far (8). Due to the diversity of phenotypes of CS, its clinical manifestation and severity do not completely depend on HLXB9 gene mutation. It is suspected that other unknown genes may also participate in the exon of mutation. Therefore, when the proband of CS is clearly diagnosed, MNX1 gene analysis and radiologic examinations of other family members are helpful to clarify the familial type or sporadic type. Twenty-three patients (72%) in our series had an MNX1 mutation. There is no obvious genotype-phenotype correlation; however, individuals with genetic mutations often have more severe phenotypes (9,10). For complete CS, whether there is MNX1 mutation or not, the evaluation should be performed by radiologic examinations. Moreover, individuals with MNX1 mutations usually have more severe phenotypes and usually accompanied by other abnormalities. Therefore, further imaging examination is needed to clarify abnormalities of spine, urogenital system, central nervous system and so on, in which situation, MRI examination is more sensitive.

Due to the diversity and severity of clinical manifestations of CS, some patients do not have any clinical presentations at the early ages; thus, CS patients are usually diagnosed at different ages (i.e., as fetal fetuses, neonates, children, and adults) (11,12). Complete CS patients with anal atresia are usually diagnosed in the neonatal period. In the present study, the age of complete CS patients ranged from 1 day to 14 years, and 50% of these patients were diagnosed in the neonatal period. Children with anal atresia with a fistula or anal stenosis were diagnosed later than those without a fistula.

CS has various symptoms, including: (I) defecation problems: the severity varies; the most serious is congenital anal atresia with or without a fistula, followed by anorectal stenosis. Hirschsprung disease can cause intractable constipation (13,14). Additionally, constipation can also be caused by the external compression of a presacral mass or tethered cord syndrome. In our series, 19 patients (59%) had defecation problems, of which 7 (21.9%) were found to have anal atresia after birth; (II) abdominal distension: This is also related to defecation disorders; difficulties in defecation lead to increased abdominal pressure. In our group, 12 patients (37.5%) had this symptom; (III) vomiting: this may be related to difficulty in defecation. On rare occasions, the central nervous system infection may cause vomiting due to increased intracranial pressure,

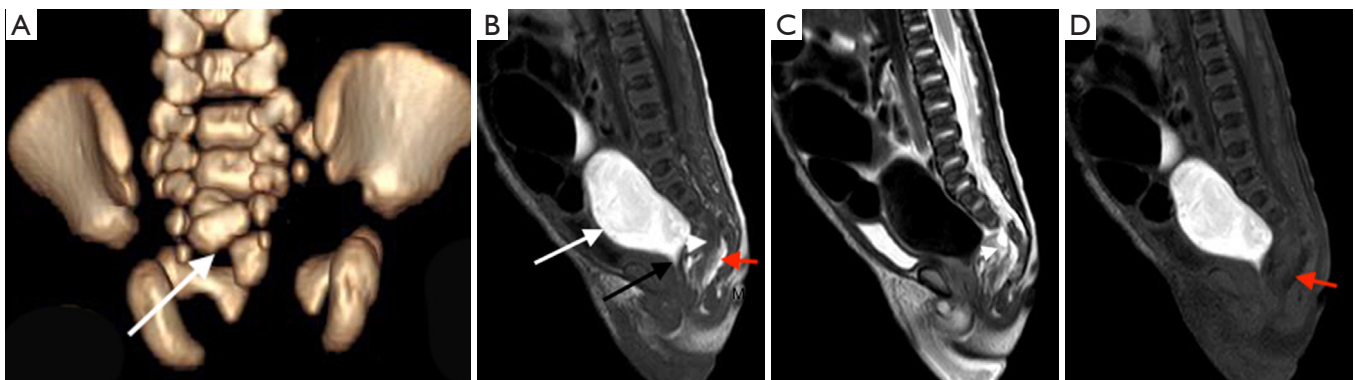


**Figure 1** A 1-day-old boy with complete CS, congenital anal atresia. (A) The CT-VR image shows type IV sacral agenesis—hemisacrum (white arrow). The sagittal T<sub>1</sub>-weighted (B) image shows the obvious dilation of the proximal rectum (white arrow), which is hyperintense because of the meconium, and the obvious narrowing of the distal rectum (black arrow). The distance from the distal rectum stenosis to the anal marker (M) can be measured to select the surgical operation method. The sagittal T<sub>1</sub>-weighted (B) and T<sub>2</sub>-weighted (C) MRI images show an anterior lipomeningocele (white arrowhead) with hyperintense fat (red arrow in B), which shows hypointensity in the fat-suppression sequence (red arrow in D). CS, Currarino syndrome; CT, computed tomography; VR, Volume Rendering; MRI, magnetic resonance imaging

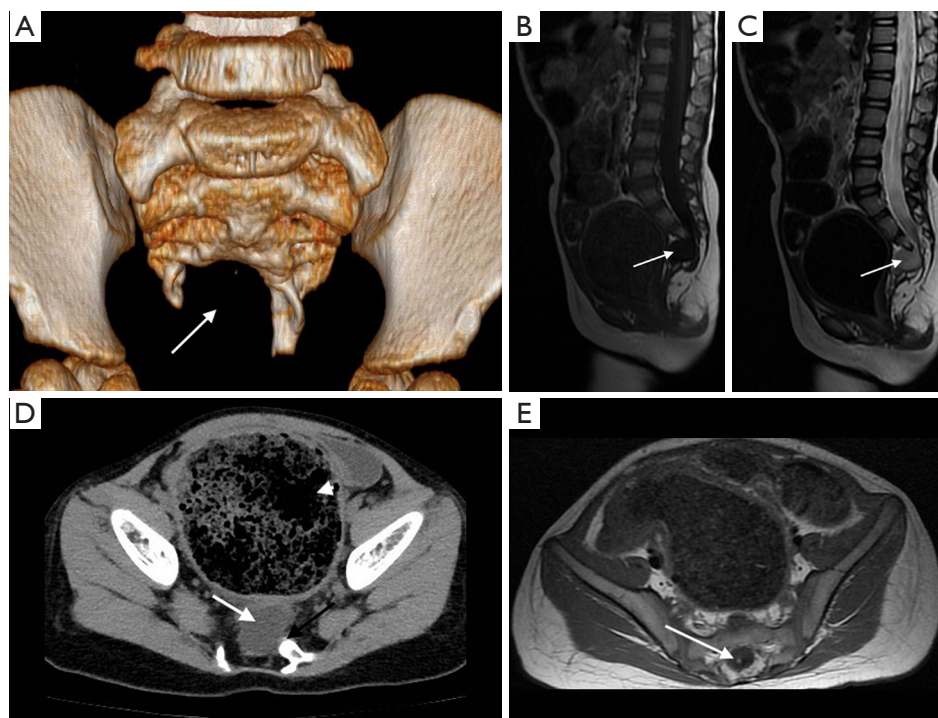


**Figure 2** A 3-year-old girl with complete CS. (A) The CT-VR image shows type IV sacral agenesis—hemisacrum (white arrow). The sagittal T<sub>1</sub>-weighted (B) and T<sub>2</sub>-weighted (C) MRI images show an anterior meningocele (white arrow) with hypointensity in the T<sub>1</sub>-weighted image and hyperintensity in the T<sub>2</sub>-weighted image. (D) The axial plain CT scan shows a low-density anterior meningocele (white arrow), sacral defect (black arrow), and obvious dilation of the sigmoid colon (white arrowhead). (E) The axial T<sub>1</sub>-weighted image shows the filum lipoma (white arrow). CS, Currarino syndrome; CT, computed tomography; VR, volume rendering; MRI, magnetic resonance imaging.

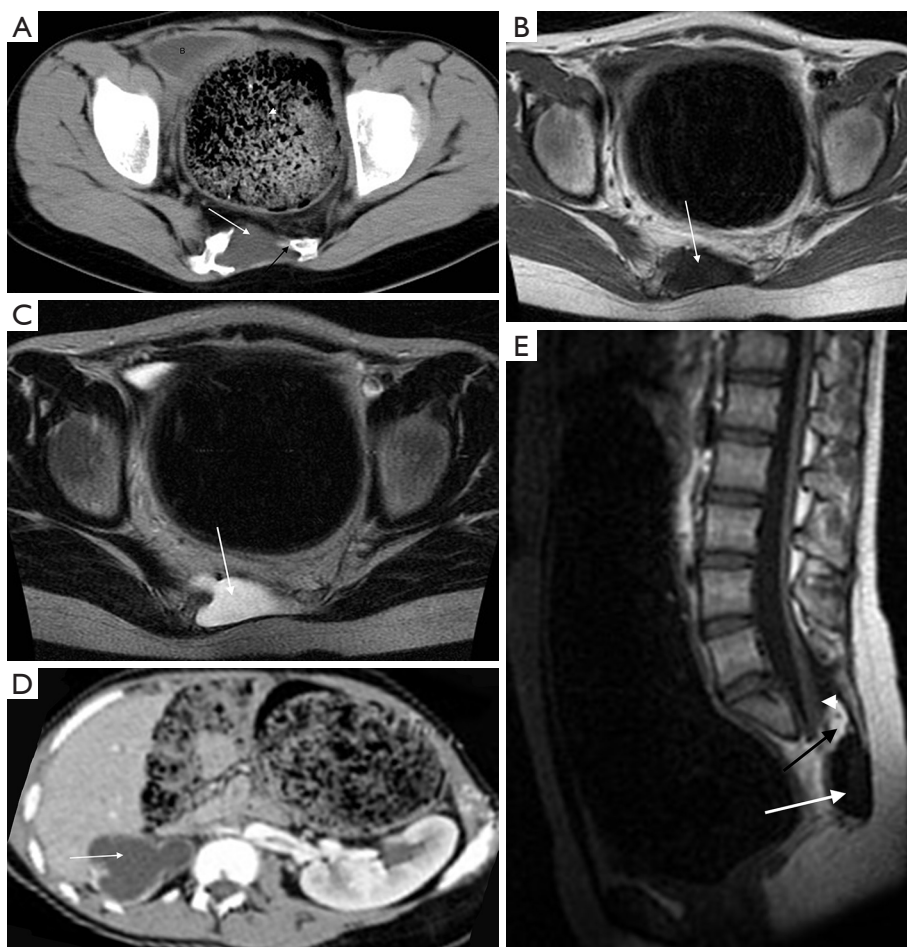


**Figure 3** A 14-year-old girl with complete CS, surgical treatment was performed for anal atresia in her neonatal period. (A) The axial plain CT scan shows a low-density anterior meningocele (white arrow), sacral agenesis (black arrow), and the obvious dilation of the colon (white arrowhead). The axial T<sub>1</sub>-weighted (B) and T<sub>2</sub>-weighted (C) MRI images show an anterior meningocele (white arrow) with hypointensity in the T<sub>1</sub>-weighted image and hyperintensity in the T<sub>2</sub>-weighted image. (D) The post-contrast CT scan shows right renal dysplasia (white arrow). (E) The sagittal T<sub>1</sub>-weighted image shows a hypointense anterior meningocele (white arrow), hyperintense intraspinal lipoma (black arrow), and a tethered cord at the level of the S1 (white arrowhead). CS, Currarino syndrome; CT, computed tomography; MRI, magnetic resonance imaging.

mainly caused by abnormal communication between the fistula and the spinal canal. Central nervous system infection is one of the most serious presentations of CS, and can even lead to death (15). Seven patients (21.9%) presented with vomiting in this study. Other less common clinical manifestations include abdominal pain, urinary dysfunction, and fever.

All the complete CS patients showed the classical triad elements (i.e., congenital ARM, sacral agenesis, and presacral mass) in our series. More than half of the patients had anal atresia, 75% with type IV—hemisacrum, nearly

half of the patients had teratomas, and 25% with anterior meningoceles. Radiography plays an important role in diagnosing complete CS, which is integral to an early diagnosis (16).

CT and MRI examinations are the main diagnostic modalities for complete CS, and have different diagnostic values. MRI is better than CT for observing congenital anal atresia. MRI can be used to observe the level of congenital anal atresia and the distance from distal rectal stenosis to the anal fossa, and to identify the type of congenital anal atresia, which provides the basis for surgical operation methods.

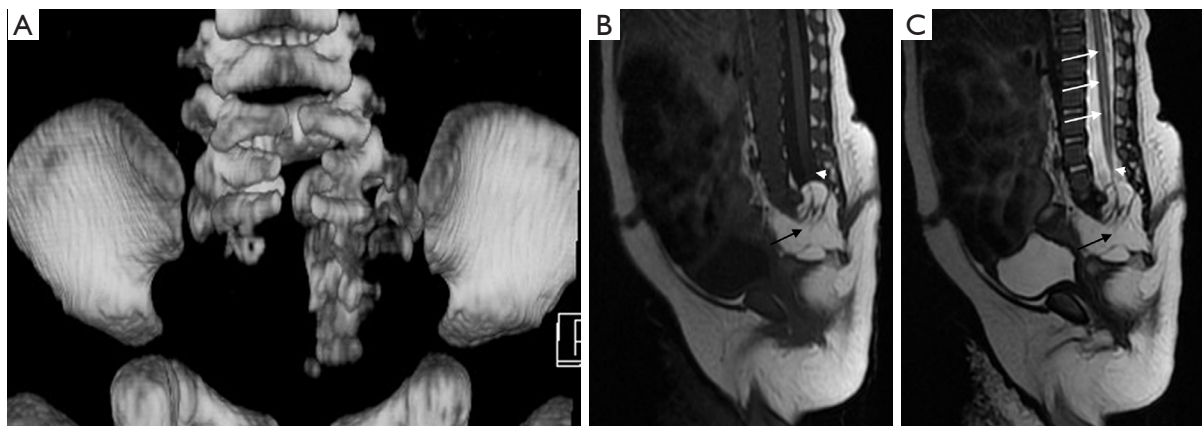


**Figure 4** A 4-month-old boy with complete CS, anal stenosis, and had dermal sinus of the lumbodorsal region. (A) The CT-VR image shows type IV sacral agenesis—hemisacrum. The sagittal T<sub>1</sub>-weighted (B) and T<sub>2</sub>-weighted (C) MRI images show the hydrosyringomyelia with hypointensity in the T<sub>1</sub>-weighted images and hyperintensity in the T<sub>2</sub>-weighted images (white arrows) at the T11-L4 level. The intraspinal lipoma shows hyperintensity both in the T<sub>1</sub>- and T<sub>2</sub>-weighted images with anterior lipomeningocele containing cauda equina (black arrow). The terminal of conus medullaris is located at the level of the L4 (white arrowhead). CS, Currarino syndrome; CT, computed tomography; VR, volume rendering; MRI, magnetic resonance imaging.

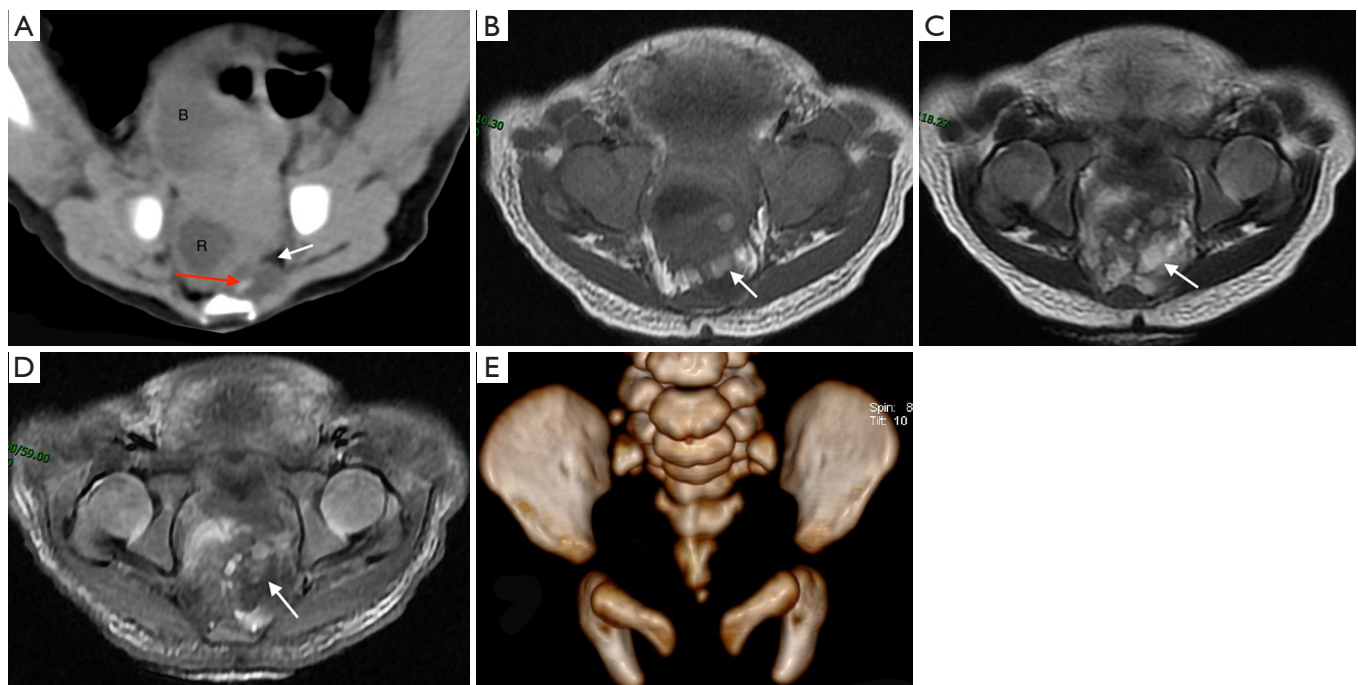


**Figure 5** A 15-day-old girl with complete CS, anal stenosis. (A) The axial plain CT scan shows a mixed density mass with fat (white arrow) and calcification (red arrow), which was confirmed to be a teratoma. The bladder (B) and rectum (R) are compressed. The axial T<sub>1</sub>-weighted (B) and T<sub>2</sub>-weighted (C) MRI images show hyperintense fat (white arrow) in the teratoma, which shows hypointensity in the fat-suppression sequence (D). (E) The CT-VR image shows type V sacral agenesis—coccyx agenesis. CS, Currarino syndrome; CT, computed tomography; VR, volume rendering; MRI, magnetic resonance imaging.

Additionally, MRI is helpful in identifying the shape, location and type of the fistula. However, for Hirschsprung disease, significant dilation of the colon and the thickened wall can be better evaluated by CT scans. Anal stenosis is usually diagnosed by a clinical digital rectal examination.

The morphologic anomalies of the sacral agenesis are easily revealed by CT multi-planer reformation (MPR) and volume rendering (VR). The most common type of sacral agenesis is the unilateral sacral defect, which may present as no unilateral sacrum at all or a partial asymmetric deformity, such as a hemisacrum with a “scimitar” or “sickle” shape (75% in our series). Additionally, CT can be used to correctly classify sacral agenesis types according to Pang’s classification. Conversely, MRI is not sensitive at detecting

mild sacral agenesis, such as type V. In our study, the sensitivity of CT for detecting sacral agenesis was 100%, which is better than that of MRI (70%).

The presacral masses of complete CS include a spectrum of anterior meningoceles, teratomas, dermoid/epidermoid or neurenteric cysts, lipomas, and other rare lesions. Teratoma is the most common true presacral tumor. Carcinoid/low-grade neuroendocrine carcinomas have rarely been reported (17). The malignant transformation of presacral masses is very rare, and only occurs in about 1% of cases (18). The majority of presacral teratomas were mature, and consisted of soft tissue components, fat, and calcification, but a few were immature. Nearly half of the presacral masses (46.9%) were true tumors in our series, and most were mature teratomas, and 1 (3.1%) was accompanied by an anterior meningocele. About half of the presacral masses (53.1%) were pseudotumors. In detecting a presacral mass, the sensitivity of MRI (91.7%) was higher than that of CT (50%). MRI was more sensitive than CT at detecting presacral mass. The size, composition, extent of the mass, and the involvement of adjacent structures could be assessed by MRI. Thus, MRI is the superior modality for assessing presacral masses, especially cystic lesions, such as dermoid/epidermoid or neurenteric cysts. MRI is also the first and best choice for evaluating a meningocele, which manifests with low signal intensity on T<sub>1</sub>WI and high signal intensity on T<sub>2</sub>WI and is connected to the spinal canal through the sacral defect. There was no difference in the detection rate of the 2 methods for presacral teratoma, as CT was sensitive to the calcification and fat in the mature teratomas.

CS may also be accompanied by other abnormalities, such as spinal dysraphisms, and urological anomalies. The probability of associated anomalies in complete CS is higher than that in incomplete CS (10). About 60% of CS patients also suffered from spinal dysraphism (19). In our series,

**Table 3** Associated anomalies of complete Currarino syndrome

Type of associated anomalies	Number of patients (%)
Spinal dysraphisms	
Tethered cord	19 (59.4)
Filum lipoma	13 (40.9)
Hydrosyringomyelia	3 (9.4)
Urological anomalies	
Hydronephrosis	5 (15.6)
Hydroureteronephrosis	2 (6.2)
Renal dysplasia	1 (3.1)
Bladder duplication	1 (3.1)
Others	
Vertebral dysmorphism	2 (6.2)
Posterior sternal hernia	1 (3.1)
Lumbosacral dermal sinus	1 (3.1)

**Table 4** The comparison between CT and MRI in detecting the classical triad elements and associated anomalies of complete Currarino syndrome

Imaging methods	Classical triad elements, n (%)			Associated anomalies, n (%)		
	Anal atresia (total 14)	Sacral anomaly (total 24)	Presacral mass (total 24)	Spinal dysraphism (total 21)	Urological anomalies (total 6)	Others (total 4)
CT	0	24 (100.0)	12 (50.0)	5 (23.8)	6 (100.0)	2 (50.0)
MRI	14 (100.0)	17 (70.1)	22 (91.7)	21 (100.0)	6 (100.0)	2 (50.0)
$\chi^2$		8.195	10.084	21.483	–	–
P value		0.005	0.002	<0.001	–	–

CT, computed tomography; MRI, magnetic resonance imaging.

associated anomalies were presented in 78% of patients, of which, consistent with the literature (19), spinal dysraphism was the most common, followed by urological anomalies. CT and MRI have different sensitivities to different kinds of concomitant anomalies. MRI has a great advantage in detecting spinal dysraphism, including tethered cord, intraspinal lipoma, and hydrosyringomyelia. In our series, the sensitivity of MRI at displaying spinal dysraphism was 100%, while the sensitivity of CT was only 23.8%. MRI was more sensitive than CT at detecting spinal dysraphism. For intraspinal abnormalities, MRI has great advantages in determining whether accompanied by tethered cord, hydrosyringomyelia, filum lipoma, diastematomyelia, and so on. For presacral anterior meningocele, MRI can identify the spinal cord and fat in it. Therefore, when complete CS is suspected, it is best to perform MRI for comprehensive evaluation. There was no significant difference in the sensitivity of the 2 methods at detecting urological anomalies and other associated anomalies.

## Conclusions

In conclusion, complete CS is a rare disorder with characteristic imaging features. CT and MRI are the main methods for diagnosing complete CS. MRI has significant advantages in diagnosing complete CS, especially in revealing the details of ARM, presacral mass, and associated spinal dysraphism. Conversely, CT is better at detecting sacral anomalies. As a non-radioactive method, MRI is the best method for diagnosing pediatric complete CS and assessing the associated abnormalities. Thus, we suggest that patients who are suspected of having complete CS with congenital ARM could be diagnosed by MRI alone.

## Acknowledgments

*Funding:* None.

## Footnote

*Reporting Checklist:* The authors have completed the MDAR checklist. Available at <https://atm.amegroups.com/article/view/10.21037/atm-21-6572/rc>

*Data Sharing Statement:* Available at <https://atm.amegroups.com/article/view/10.21037/atm-21-6572/dss>

*Conflicts of Interest:* All authors have completed the

ICMJE uniform disclosure form (available at <https://atm.amegroups.com/article/view/10.21037/atm-21-6572/coif>). The authors have no conflicts of interest to declare.

*Ethical Statement:* The authors are accountable for all aspects of the work in ensuring that questions related to the accuracy or integrity of any part of the work are appropriately investigated and resolved. All procedures performed in this study involving human participants were in accordance with the Declaration of Helsinki (as revised in 2013). The study was approved by the Ethics Committee of Tianjin Children's Hospital (No. 2016021) and Wuhan Children's Hospital (No. 2020RO15-E01). Individual consent for this retrospective analysis was waived.

*Open Access Statement:* This is an Open Access article distributed in accordance with the Creative Commons Attribution-NonCommercial-NoDerivs 4.0 International License (CC BY-NC-ND 4.0), which permits the non-commercial replication and distribution of the article with the strict proviso that no changes or edits are made and the original work is properly cited (including links to both the formal publication through the relevant DOI and the license). See: <https://creativecommons.org/licenses/by-nc-nd/4.0/>.

## References

1. Currarino G, Coln D, Votteler T. Triad of anorectal, sacral, and presacral anomalies. *AJR Am J Roentgenol* 1981;137:395-8.
2. Belloni E, Martucciello G, Verderio D, et al. Involvement of the HLXB9 homeobox gene in Currarino syndrome. *Am J Hum Genet* 2000;66:312-9.
3. Kumar B, Sinha AK, Kumar P, et al. Currarino syndrome: Rare clinical variants. *J Indian Assoc Pediatr Surg* 2016;21:187-9.
4. Gupta S, Chunnilal J, Mehrotra M, et al. Recurrent Abortion and Tethered Cord Syndrome Caused by Anterior Sacral Meningocele: A Report of a Rare Case with a Review of the Literature. *World Neurosurg* 2017;101:815.e5-7.
5. Pang D. Sacral agenesis and caudal spinal cord malformations. *Neurosurgery* 1993;32:755-78; discussion 778-9.
6. Lynch SA, Bond PM, Copp AJ, et al. A gene for autosomal dominant sacral agenesis maps to the holoprosencephaly region at 7q36. *Nat Genet* 1995;11:93-5.
7. Ross AJ, Ruiz-Perez V, Wang Y, et al. A homeobox gene,

- HLXB9, is the major locus for dominantly inherited sacral agenesis. *Nat Genet* 1998;20:358-61.
8. Merello E, De Marco P, Ravegnani M, et al. Novel MNX1 mutations and clinical analysis of familial and sporadic Currarino cases. *Eur J Med Genet* 2013;56:648-54.
  9. Lee S, Kim EJ, Cho SI, et al. Spectrum of MNX1 Pathogenic Variants and Associated Clinical Features in Korean Patients with Currarino Syndrome. *Ann Lab Med* 2018;38:242-8.
  10. Costanzo S, Spaccini L, Pio L, et al. Currarino syndrome: does the presence of a genetic anomaly correlate with a more severe phenotype? A multicentre study. *J Pediatr Surg* 2017;52:1591-6.
  11. Caro-Domínguez P, Bass J, Hurteau-Miller J. Currarino Syndrome in a Fetus, Infant, Child, and Adolescent: Spectrum of Clinical Presentations and Imaging Findings. *Can Assoc Radiol J* 2017;68:90-5.
  12. Akay S, Battal B, Karaman B, et al. Complete currarino syndrome recognized in adulthood. *J Clin Imaging Sci* 2015;5:10.
  13. Bou-Assaly W, Illner A, Delaney L, et al. AJR Teaching File: child with chronic constipation. *AJR Am J Roentgenol* 2007;189:S29-31.
  14. Paradies G, Zullino F, Orofino A, et al. Unusual presentation of sacrococcygeal teratomas and associated malformations in children: clinical experience and review of the literature. *Ann Ital Chir* 2013;84:333-46.
  15. Al Qahtani HM, Suliman Aljoqiman K, Arabi H, et al. Fatal Meningitis in a 14-Month-Old with Currarino Triad. *Case Rep Radiol* 2016;2016:1346895.
  16. Pérez Vega-Leal C, Sainz Gómez C, Ubis Rodríguez E, et al. Radiological findings in Currarino syndrome. *Radiologia* 2013;55:233-8.
  17. Colombo F, Janous P, Buxton N. Carcinoid transformation of presacral dermoid cyst in patient with currarino syndrome: a case report. *Br J Neurosurg* 2019;33:285-6.
  18. Dirix M, van Becelaere T, Berkenbosch L, et al. Malignant transformation in sacrococcygeal teratoma and in presacral teratoma associated with Currarino syndrome: a comparative study. *J Pediatr Surg* 2015;50:462-4.
  19. Kole MJ, Fridley JS, Jea A, et al. Currarino syndrome and spinal dysraphism. *J Neurosurg Pediatr* 2014;13:685-9.
- (English Language Editor: L. Huleatt)

**Cite this article as:** Chen J, Zheng N, Wang C, Shao J, Qi X, Xie Y, Zhang Q. Characterization of complete Currarino syndrome in pediatrics—a comparison between CT and MRI. *Ann Transl Med* 2022;10(2):63. doi: 10.21037/atm-21-6572